Intrinsic ICI-free Alamouti Coded FBMC

Dongjun Na and Kwonhue Choi, *Senior Member, IEEE*

***Abstract*—Applying Alamouti code to FBMC (filter bank multicarrier) is a challenging issue due to the intrinsic inter-antenna inter-carrier interference (ICI), which does not exist in Alamouti coded OFDM. We propose a frequency reversal Alamouti coded scheme for FBMC. As the frequency reversal symbol arrangement in itself cannot handle the inter-antenna ICI, we carefully consider the signal structure of FBMC and specify the additional requirements to satisfy self ICI cancelation property. Only with a simple signal modification in the transmitter and the typical Alamouti decoding in the receiver, the proposed scheme achieves ideal (ICI-free) Alamouti code performance if the fading is locally flat over the Alamouti coded block. By properly dividing the total bandwidth into multiple blocks, the proposed scheme achieves near ICI-free performance for the multi-path fading channels.**

***Index Terms*—FBMC (filter bank multicarrier), Alamouti code, Offset QAM (OQAM), 5G systems, Millimeter(mm) wave.**

I. Introduction

Unlike OFDM, FBMC undergoes inter-antenna ICI. This is due to the unique feature of FBMC that the received phase difference between the TX antennas introduces ICI between the subcarrier transmitted from one TX antenna and the adjacent sub-carriers transmitted from another TX antenna[1, 2]. This intrinsic inter-antenna ICI makes it a challenging issue to apply Alamouti code to FBMC system. Recently, a few studies have been made to tackle this issue. In [2], CDMA-based approach has been studied to suppress the inter-antenna ICI. In [3], an iterative interference cancelation approach has been employed. In [4], multiple IDFT/DFT blocks are added to the transmitter and the receiver to get rid of the intrinsic interference of FBMC signal. All these approaches require the considerable computation complexities in the transmitter or the receiver side.

In [5], a simple block Alamouti coded scheme has been proposed for FBMC. The ideal performance of this scheme is based on the static fading assumption over the block and thus, this scheme undergoes severe degradation as the Doppler rate increases. Also, due to its time reversal (TR) block structure, decoding latency is inevitable. These shortcomings become more critical in the 5G systems for which the FBMC is one of the candidate modulations. This is because in the 5G systems, the large Doppler rate by using mm-Wave band is highly expected and the ultra low latency is one of the key requirements.

This research was supported in part by Basic Science Research Program through the National Research Foundation (2015R1D1A3A01015970) and the Information Technology Research Center support program (IITP-2016-R2718-16-0035) supervised by the Institute for Information & communications Technology Promotion funded by the Ministry of Science, ICT and Future Planning, Korea.

D. Na and K. Choi(Corresponding author) are with Dept. of ICE, Yeungnam University, Korea. e-mail: nadj2964,gonew@ynu.ac.kr.

Through a close investigation, we found a similarity in inter-antenna ICI term structures between the OFDM signal with distributed TX antennas[6, 7] and the FBMC signal, i.e., Hermitian symmetry in frequency axis. This inspires us a possibility that the frequency reversal scheme may be applied to Alamouti coded FBMC and we may achieve self ICI cancelation as done in FADAC-OFDM[6]. Meanwhile, unlike FADAC-OFDM, a purely frequency reversal Alamouti coded FBMC can not achieve the self ICI cancelation property but some modifications should be added to meet the unique signal structure of the FBMC. Consequently, the proposed frequency reversal scheme needs a very simple signal modification in the TX side and nothing but the typical Alamouti decoding in the RX side.

II. Frequency Reversal Alamouti coded FBMC

A. Transmit signal structure

The total N_c subcarriers are partitioned into the multiple blocks with size N_F. Each block is individually structured as Fig. 1. Each block consists of two half blocks which contain $N_F/2-1$ data symbols followed by one zero(null). In the left half block, the real-valued data symbols are packed and in the right half block, their Alamouti coded pairs are packed in the frequency reversal manner. By the null subcarriers in between the blocks, the blocks are mutually orthogonalized. Hence, hereafter, we consider only one block's signal for simplicity without loss of generality.

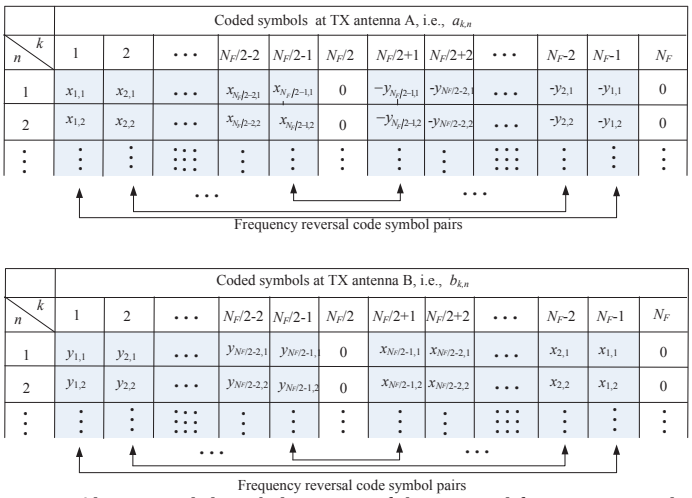

Fig. 1. Alamouti coded symbol mapping of the proposed frequency reversal scheme

Denote $(x_{k,n}, y_{k,n})$ as the real valued data symbol pair, then they will be Alamouti coded and then transmitted at (k, n)th and $(N_F - k, N_F)$th slots in the subcarrier-time frame in Fig. 1. Denote $a_{k,n}$ and $b_{k,n}$ as the Alamouti coded symbol transmitted at (k, N_F)-th slot of the subcarrier-time matrix

from the TX antenna A and B, respectively, then the coded symbol pairs in the frequency reversal positions at each TX antenna, i.e., $(a_{k,n},\ a_{N_F-k,n})$ and $(b_{k,n},\ b_{N_F-k,n})$ form the Alamouti code structure as follows:

$$\begin{pmatrix} a_{k,n} & a_{N_F-k,n} \\ b_{k,n} & b_{N_F-k,n} \end{pmatrix} = \begin{pmatrix} x_{k,n} & -y_{k,n} \\ y_{k,n} & x_{k,n} \end{pmatrix}. \quad (1)$$

Subsequently going through the typical FBMC modulation rule, the following signals are transmitted from two TX antennas:

$$s_a(t) = \sum_{l=1}^{N_F-1}\sum_{m=-\infty}^{\infty} a_{l,m}\zeta_{l,m}p\left(t-\tfrac{T}{2}m\right)e^{j\frac{2\pi lt}{T}}, \quad (2)$$

$$s_b(t) = \sum_{l=1}^{N_F-1}\sum_{m=-\infty}^{\infty} b_{l,m}\zeta_{l,m}p\left(t-\tfrac{T}{2}m\right)e^{j\frac{2\pi lt}{T}} \quad (3)$$

where T is the symbol duration of the OQAM signal and $p(t)$ is a frequency-localized FBMC pulse such as PHYDYAS pulse[1, 8] or IOTA pulse[2, 8] with unit energy.

The term $\zeta_{l,m}$ is the phase shift term alternating between $1(\text{or } -1)$ and $j(\text{or } -j)$ in both of time and frequency axes to form the OQAM signal from the real valued data sequences $a_{l,m}$ and $b_{l,m}$. In the left half subcarriers, i.e., for $1 \le l \le N_F/2-1$, $\zeta_{l,m}$ is set to satisfy the following rule which is a basic requirement for FBMC modulation[3]:

$$\zeta_{l,m} = \begin{cases} 1\ (\text{or } -1) & \text{if } l+m = \text{even}, \\ j\ (\text{or } -j) & \text{if } l+m = \text{odd}. \end{cases} \quad (4)$$

As there is no constraint on the polarities, there exist numerous patterns which satisfy the rule in (4).

On the other hand, in the right half subcarriers, i.e., for $\zeta_{N_F-l,m}$ with $1 \le l \le N_F/2-1$, the proposed scheme has a requirement that they should be set to the conjugate of their frequency reversal counter parts in the left half subcarrier, i.e.,

$$\zeta_{N_F-l,m} = \zeta_{l,m}^*. \quad (5)$$

In addition to the frequency reversal symbol arrangement, the phase shifting rule in (5) and the null subcarrier insertion in between the half parts of each block are the essential requirements to accomplish the desired property of the proposed scheme, i.e, ICI-free performance. The detailed proof is given in the next subsection.

B. Received signal and demodulation

The received signal of the considered block is modeled as

$$r(t) = h_a s_a(t) + h_b s_b(t) + n(t) \quad (6)$$

where h_a and h_b denote the overall channel gain within the block from TX antenna A and B, respectively including the multiplicative fading gains and $n(t)$ is the background noise whose power spectral density is set to $N_0/2$.

The received sample for (k,n)-th frequency-time element $r_{k,n}$ is calculated by FBMC demodulation as follows:

$$r_{k,n} = \int_{-\infty}^{\infty} r(t)\zeta_{k,n}^* p\left(t-\tfrac{nT}{2}\right)e^{-j\frac{2\pi kt}{T}}dt. \quad (7)$$

Then, the typical combining for Alamouti code is employed. Denote $d_{k,n}^{(x)}$ and $d_{k,n}^{(y)}$ as the decision variables for the data symbols $x_{k,n}$ and $y_{k,n}$, respectively then, they are obtained as follows:

$$d_{k,n}^{(x)} = \Re\left[h_a^* r_{k,n} + h_b r_{N_F-k,n}^*\right], \quad (8)$$

$$d_{k,n}^{(y)} = \Re\left[h_b^* r_{k,n} - h_a r_{N_F-k,n}^*\right] \quad (9)$$

where $\Re[z]$ denotes the real part of z.

Substituting (2) and (3) into (6) and then into (7) and performing some tedious maths, we can write $r_{k,n}$ as follows:

$$r_{k,n} = h_a\sum_{l=-L}^{L}\sum_{m=-M}^{M}F_{l,m}\zeta_{k+l,n+m}\zeta_{k,n}^*(-1)^{nl}a_{k+l,n+m} + h_b\sum_{l=-L}^{L}\sum_{m=-M}^{M}F_{l,m}\zeta_{k+l,n+m}\zeta_{k,n}^*(-1)^{nl}b_{k+l,n+m} + w_{k,n} \quad (10)$$

where $F_{l,m} = \int_{-\infty}^{\infty} p\left(t-\frac{mT}{2}\right)p(t)e^{-j\frac{2\pi lt}{T}}dt$ and $w_{k,n}$ corresponds to the noise component in the received sample $r_{k,n}$ and is a zero mean complex Gaussian random variable with the variance equal to the background noise density $N_0/2$.

In the literature, $F_{l,m}$ is called the trans-multiplexer impulse response of the pulse $p(t)$. Note that for the FBMC application, the pulse $p(t)$ should be localized in the frequency domain as well as the time domain and thus, $F_{l,m}$ is approximately 0 for $|l| > L$ or $|m| > M$. This is why the summation ranges in (10) are limited to $-L \le l \le L$ and $-M \le m \le M$. For reference, for PHYDYAS pulse, $L = 1$ and $M = 3$ and for IOTA pulse, $L = 2$ and $M = 3$[8].

Let us define

$$F_{l,m}^{(k,n)} \triangleq F_{l,m}\zeta_{k+l,n+m}\zeta_{k,n}^*(-1)^{nl} \quad (11)$$

which implies the overall interference coefficient of the symbol at $(k+l, n+m)$-th frequency time slot to the symbol at (k,n)-th frequency time slot in (10). Due to the characteristics of the FBMC pulse shaping filter and the alternating phase terms by the rules (4), the following property holds:

$$\text{Property I:}\quad \Re\left[F_{l,m}^{(k,n)}\right] = \delta_l\delta_m, \quad (12)$$

and by the property $F_{-l,m} = F_{l,m}^*$, i.e., Hermitian symmetry w.r.t. l and the proposed phase shifting rule in (5), the following property holds:

$$\text{Property II:}\quad F_{-l,m}^{(N_F-k,n)} = F_{l,m}^{*(k,n)}. \quad (13)$$

By using (11) and substituting (1) into (10), we have

$$r_{k,n} = h_a\underbrace{\sum_{l=-L}^{L}\sum_{m=-M}^{M}F_{l,m}^{(k,n)}x_{k+l,n+m}}_{\triangleq U} + h_b\underbrace{\sum_{l=-L}^{L}\sum_{m=-M}^{M}F_{l,m}^{(k,n)}y_{k+l,n+m}}_{\triangleq V} + w_{k,n}, \quad (14)$$

$$r_{N_F-k,n} = h_a\underbrace{\sum_{l=-L}^{L}\sum_{m=-M}^{M}F_{l,m}^{(N_F-k,n)}\times(-y_{k-l,n+m})}_{\triangleq W} + h_b\underbrace{\sum_{l=-L}^{L}\sum_{m=-M}^{M}F_{l,m}^{(N_F-k,n)}x_{k-l,n+m}}_{\triangleq Z} + w_{N_F-k,n}. \quad (15)$$

For compact presentations in the subsequent derivations, the double summation terms in (14) and (15) are denoted by the single letters under the lines.

Substituting (14) and (15) into (8), we have

$$d_{k,n}^{(x)} = \Re\left[h_a^*(h_aU + h_bV) + h_b(h_aW + h_bZ)^*\right] + n_{k,n}^{(x)} = |h_a|^2\Re[U] + |h_b|^2\Re[Z^*] + \Re\left[h_a^*h_b(V+W^*)\right] + n_{k,n}^{(x)} \quad (16)$$

where $n_{k,n}^{(x)} = \Re[h_a^*w_{k,n} + h_bw_{N_F-k,n}^*]$ and denotes the noise component in the decision variable in $d_{k,n}^{(x)}$. Using property I in (12), the term $\Re[U]$ is derived as:

$$\Re[U] = \sum_{l=-L}^{L}\sum_{m=-M}^{M}\delta_l\delta_m x_{k+l,n+m} = x_{k,n} \quad (17)$$

and similarly,

$$\Re[Z^*] \quad = \quad x_{k,n}. \tag{18}$$

The term W^* is written as

$$W^* \quad = \quad \left[\sum_{l=-L}^{L}\sum_{m=-M}^{M} F_{-l,m}^{(N_F-k,n)} \times (-y_{k+l,n+m})\right]^* \tag{19}$$

and by Property II in (13),

$$\begin{aligned} W^* &= \left[\sum_{l=-L}^{L}\sum_{m=-M}^{M} F_{l,m}^{*(k,n)} \times (-y_{k+l,n+m})\right]^* \\ &= -\sum_{l=-L}^{L}\sum_{m=-M}^{M} F_{l,m}^{(k,n)} y_{k+l,n+m} = -V. \end{aligned} \tag{20}$$

Consequently, substituting (17), (18) and (20) into (16), we have

$$d_{k,n}^{(x)} = \left(|h_a|^2 + |h_b|^2\right) x_{k,n} + n_{k,n}^{(x)}. \tag{21}$$

Similarly,

$$d_{k,n}^{(y)} = \left(|h_a|^2 + |h_b|^2\right) y_{k,n} + n_{k,n}^{(y)} \tag{22}$$

where $n_{k,n}^{(y)}$ denotes the noise component in the decision variable in $d_{k,n}^{(y)}$. Note that the signal terms and the noise terms in the decision variables (21) and (22) have the same distributions as the case with the ideal Alamouti decoding, i.e., the ICI-free case.

III. Simulation Results

A. Verification of ICI cancelation property

Recall that in (6), h_a and h_b are set to be constant, i.e., we assumed that the channel fading is locally flat over the frequency reversal coded block. However, as the channel selectivity increases, this assumption becomes less realistic and thus, the ICI is not perfectly canceled. In order to see how much the performance of the proposed scheme gets off from the ideal (ICI-free) Alamouti coded case, we simulated the BER (bit error rate) of the proposed scheme under the various multi-path channels. The number of multi-paths L is set to 5. The first arrival path's delay is set to 0 and the remaining $L-1$ multi-paths are uniformly distributed on [0 τ_{max}] where τ_{max} denotes maximum delay range. The path power is set to exponentially decay from 0 when $t = 0$ to -20 dB when $t = \tau_{max}$. The subcarrier spacing $f_\Delta(= 1/T)$ is set to 15 kHz.

Fig. 2 shows the simulated BERs (bit error rates) according to the maximum delay range τ_{max} and the frequency reversal block size N_F. Basically, it is common to all curves that as τ_{max} decreases, the BERs of the proposed scheme converge to that of the ideal (ICI-free) Alamouti code. This confirms the perfect self ICI cancelation property of the proposed scheme for the locally flat channel that we have analytically shown in the previous section. Due to less frequency localization of the IOTA pulse compared to the PHYDYAS pulse[8], the IOTA pulse results in the negligibly increased BERs compared to the PHYDYAS pulse in low BER region.

As τ_{max} increases, the BERs gradually increase. This is because the fading coefficients at each subcarrier within the coded block deviate from the constant value due to the frequency selectivity and thus, the self ICI cancelation does not work. Meanwhile, if we properly decrease N_F according to

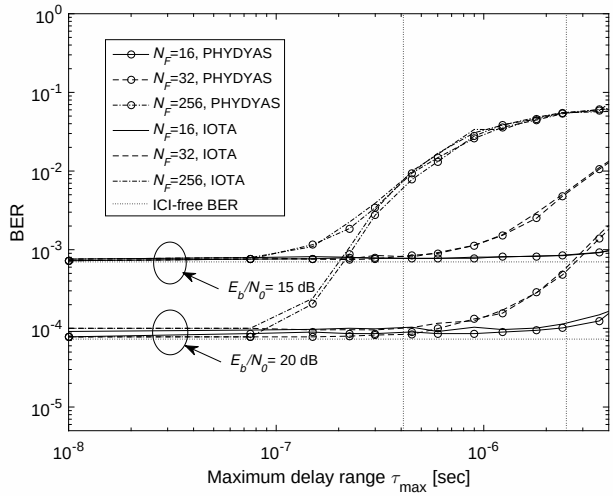

Fig. 2. Simulated BERs of the proposed FR scheme under multipath fading channels, E_b/N_0=15 dB and 20 dB, OQPSK.

τ_{max}, the proposed scheme can still achieve near ICI-free performance. For example, for τ_{max}=0.41μs which approximates ITU-R Pedestrian-A channel model[9], the proposed scheme with N_F=32 achieves near ICI-free performance at the cost of 6.25%(=2/N_F) null data overhead. For τ_{max}=2.5μs which approximates ITU-R Vehicular-A channel model, the proposed scheme with N_F=16 achieves the BERs little above ICI-free level at the cost of 12.5% null data overhead.

B. Comparison with the time reversal scheme

To see the dependency of BER performance on time selectivity as well as frequency selectivity of the fading channel, we simulate time varying multipath fading. The Doppler spectrum of each path follows Jakes model. In Fig. 3, we plot the simulated BERs over (τ_{max}, R_D(=Doppler rate)) plane for OQPSK and 16-OQAM. Unlike the dependency on frequency selectivity, the performance of the proposed scheme shows almost no difference against R_D. This is because even with high R_D, say 150 Hz, the fading cycle roughly corresponds to 75 FBMC symbol duration and thus, fading is quasi-static over each FBMC symbol duration.

For comparison with the TR scheme in [5], the TR scheme is also simulated under the identical fading channels and the simulated BERs are overlaid in Fig. 3 where N_T denotes the time reversal block length. For fair comparison under the same data rate basis, we need to set N_T and N_F so that the data loss by the null symbols are identical to both schemes. Note that the TR scheme needs 4 null symbols out of N_T symbols (=2 null symbols ahead of each half block) to avoid inter half block interference[5]. Thus, the null data overhead is $4/N_T$. On the other hand, the proposed FR scheme needs two null subcarrier out of N_F subcarriers and thus, the null data overhead is $2/N_F$. Therefore, we set $N_T = 2N_F$ for the fair data rate comparison in each subplot of Fig. 3.

There is a partial analogy between the TR scheme and the proposed FR scheme as they both rely on the reversal arrangement in time and frequency, respectively. This analogy makes it intuitive that the TR scheme will have the switched

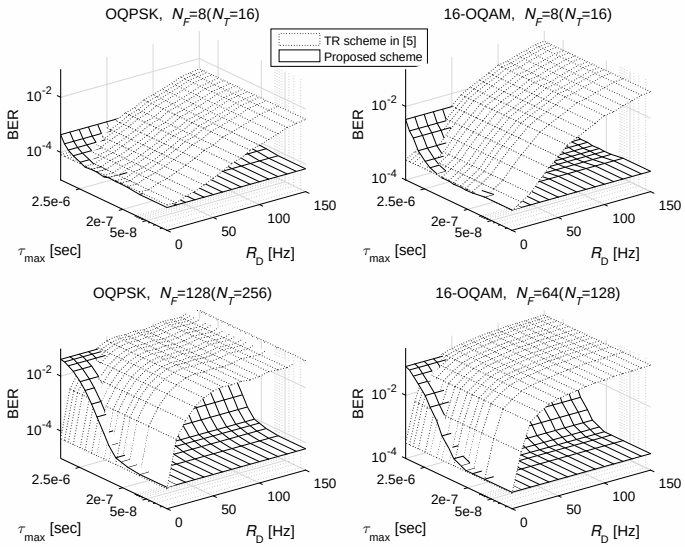

Fig. 3. Simulated BERs according to maximum delay range and Doppler rate for OQPSK and 16-OQAM with E_b/N_0=20dB, PHYDYAS pulse.

trends in time and frequency domains from those of the proposed FR scheme. Fig. 3 confirms this intuition. Firstly, the BERs of the TR scheme show almost no difference against τ_{max}. Secondly, as R_D increases, the BERs of the TR scheme increase. Note that even with practical range of R_D, the BERs of the TR scheme increase to the unacceptable level and the degradation is more emphasized for larger N_T. Similarly to decreasing N_F of the proposed FR scheme to avoid the BER increase, it is shown that the TR scheme can somehow avoid the BER increase by decreasing N_T. By the time-frequency switched trend in Fig.3, we draw a rather trivial trade-off as follows. For time varying and less frequency selective fading, the proposed FR scheme outperforms the TR scheme. On the other hand, for more frequency selective but very slow fading (left corners of each subplot in Fig.3), the TR scheme outperforms the proposed scheme.

As the FBMC is one of the candidate modulations for the 5G system, it is timely and meaningful to assess the suitability of the proposed scheme to the 5G system. For the prospective 5G wireless channel, the tradeoff mentioned above becomes meaningless and it rather concludes that the proposed scheme is definitely preferred to the TR scheme. The mm-Wave band has been recently considered to be used in 5G wireless systems[10]. From Figure 15 and Figure 16 in [10], we can roughly set τ_{max}=200 ns and 50 ns for 28 GHz and 38 GHz bands, respectively. Meanwhile, R_D at these bands significantly increases as R_D is proportional to the carrier frequency. For instance, even with the pedestrian speed of 4 km/h, R_D is approximately 104 Hz and 141 Hz for 28 GHz and 38 GHz, respectively. In this region of (τ_{max}, R_D) (the area around the right corners of each subplot in Fig. 3), the proposed scheme with N_F as large as 128 still achieves near ICI-free performance with null data overhead=1.56% which is negligible. On the other hand, the TR scheme with N_T as small as 16 still has the unacceptable BER levels despite null data overhead=12.5%.

Another key requirement in 5G systems is ultra low latency. In the proposed scheme, the Alamouti coded pairs are split into frequency reversal subcarriers of the same FBMC symbol and thus, just one FBMC symbol duration is needed for Alamouti decoding. On the other hand, in the TR scheme, the Alamouti coded pairs are split into two remote FBMC symbols in time reversal manner and we cannot perform Alamouti decoding of the coded pairs located at the both ends of the time reversal block until the entire symbols in the block are demodulated. Therefore, the TR scheme undergoes worst decoding latency equal to N_T symbol duration. If we decrease N_T for small latency, it ends up with high null data overhead because the two out of N_T symbols are null symbols. Consequently, the TR scheme basically bears the tradeoff between decoding latency and null data overhead. On the other hand, the proposed scheme is free from this tradeoff.

IV. Conclusions

The proposed frequency reversal Alamouti coding scheme for FBMC achieves near ICI-free performance. Moreover, the proposed scheme requires very simple signal modifications and negligible computation complexity compared to the existing schemes. In the light of these features, it is expected that the proposed scheme will be a promising candidate of Alamouti coding for the future FBMC-based systems.

References

[1] Bellanger, M., et al., "FBMC physical layer: a primer," PHYDYAS, January (2010).

[2] Chrislin Lele, Pierre Siohan and Rodolphe Legouable. "The alamouti scheme with CDMA-OFDM/OQAM," *EURASIP Journal on Advances in Signal Processing* 2010, pp. 1-13.

[3] Rostom Zakaria and Didier Le Ruyet, "A novel filter-bank multicarrier scheme to mitigate the intrinsic interference: application to MIMO systems," *IEEE Trans. on Wirel Commun.*, vol. 11 no. 3, March 2012, pp. 1112-1123.

[4] Rostom Zakaria and Didier Le Ruyet, "On interference cancellation in Alamouti coding scheme for filter bank based multicarrier systems," *ISWCS*, 2013. pp. 1-5.

[5] Markku Renfors, et al., "A block-Alamouti scheme for filter bank based multicarrier transmission," *European Wireless Conference*, 2010, pp. 1031-1037.

[6] Bong-seok Kim and Kwonhue Choi, "FADAC-OFDM: Frequency-asynchronous distributed alamouti-coded OFDM, " , *IEEE Trans. on Veh. Tech.*, vol. 64, no 2, 2015, pp. 466-480.

[7] Kwonhue Choi "Inter-carrier interference-free Alamouti-coded OFDM for cooperative systems with frequency offsets in non-selective fading environments," *IET Commun.*, vol. 5, no. 15, pp. 2125–2129, Oct. 2011.

[8] Zakaria, Rostom and Didier Le Ruyet. "Partial interference cancellation with maximum likelihood sequence detection in FBMC spatial multiplexing system," *EURASIP Journal on Advances in Signal Processing* April 2016.

[9] ITU-R M.1225, "Guidelines for Evaluations of Radio Transmission Technologies for IMT-2000," 1997.

[10] Theodore S. Rappaport, et al., "Millimeter wave mobile communications for 5G cellular: It will work!," *IEEE Access*, May 2013, pp. 335-349.